

Arctic warming, moisture increase and circulation changes observed in the Ny-Ålesund homogenized radiosonde record

Marion Maturilli¹  · Markus Kayser¹

Received: 2 June 2015 / Accepted: 1 July 2016
© Springer-Verlag Wien 2016

Abstract Radiosonde measurements obtained at the Arctic site Ny-Ålesund (78.9°N, 11.9°E), Svalbard, from 1993 to 2014 have been homogenized accounting for instrumentation discontinuities by correcting known errors in the manufacturer provided profiles. The resulting homogenized radiosonde record is provided as supplementary material at <http://doi.pangaea.de/10.1594/PANGAEA.845373>. From the homogenized data record, the first Ny-Ålesund upper-air climatology of wind, temperature and humidity is presented, forming the background for the analysis of changes during the 22-year period. Particularly during the winter season, a strong increase in atmospheric temperature and humidity is observed, with a significant warming of the free troposphere in January and February up to 3 K per decade. This winter warming is even more pronounced in the boundary layer below 1 km, presumably amplified by mesoscale processes including e.g. orographic effects or the boundary layer capping inversion. Though the largest contribution to the increasing atmospheric water vapour column in winter originates from the lowermost 2 km, no increase in the contribution by specific humidity inversions is detected. Instead, we find an increase in the humidity content of the large-scale background humidity profiles. At the same time, the tropospheric flow in winter is found to occur less frequent from northerly directions and to the same amount more frequent from the South. We conclude that changes in the atmospheric circulation lead to an enhanced advection of warm and moist air from lower latitudes to the Svalbard region in the winter season, causing the

warming and moistening of the atmospheric column above Ny-Ålesund, and link the observations to changes in the Arctic Oscillation.

1 Introduction

Various processes contributing to Arctic amplification cause global warming to be effectively larger in the Arctic region (e.g. Serreze and Barry 2011). The amplifying feedback mechanisms are based on atmosphere-cryosphere-ocean interactions with the diminishing Arctic sea ice in the leading role. The interplay of the retreating sea ice cover and the atmosphere includes radiation-based concepts as the snow/ice-albedo feedback, with less high reflective sea ice (or snow cover) exposing more open water (or dark underlying) surface to absorb solar radiation and further trigger the warming and melting. Further reduction in Arctic albedo is related to soot on snow and on sea ice linked to fossil burning (Hansen and Nazarenko 2004; Marks and King 2013) and heat-absorbing black carbon aerosols in the atmosphere (Shindell and Faluvegi 2009). More importantly, the changes in sea ice extent affect the vertical heat fluxes between the Arctic Ocean and the overlying atmosphere (Serreze et al. 2009; Screen and Simmonds 2010). Considering the impact of the extended open water surface on the latent heat fluxes, related changes in cloud cover and atmospheric water vapour content affect the downward longwave (LW) radiation flux (Francis and Hunter 2006; Schweiger et al. 2008). Moreover, circulation changes also increase the meridional transport of water vapour to the Arctic with impact on the LW radiation (Doyle et al. 2011; Park et al. 2015). In addition, changes in the atmospheric and oceanic meridional heat transport have a share in Arctic warming (Graversen et al. 2008; Chylek et al. 2009). In fact, the vertical structure of the recent Arctic warming evidences

✉ Marion Maturilli
marion.maturilli@awi.de

¹ Alfred Wegener Institute, Helmholtz Centre for Polar and Marine Research, Telegrafenberg A43, 14473 Potsdam, Germany

temperature amplification well above the surface for most part of the year, explained by atmospheric energy transport into the Arctic (Graversen et al. 2008). In the vertical, the presence of a temperature inversion in the clear-sky winter atmosphere contributes to the warming of the atmospheric layers below by additional downward LW radiation and to the damping of LW cooling to space (Bintanja et al. 2011). In addition, the predominant presence of specific humidity inversions in the Arctic influences LW radiation in clear-sky conditions (Devasthale et al. 2011). In addition, specific humidity inversions have implications for cloud growth and persistence (Solomon et al. 2011; Sedlar et al. 2012). Though the Arctic atmosphere is particularly dry, water vapour contributes most of all gases to LW emission (Curry et al. 1995) and creates supersaturations that maintain clouds causing additional LW forcing (Shupe and Intrieri 2004). Changes in water vapour content are thus expected to have a strong impact on the Arctic climate system.

In our study, we focus on observations at Ny-Ålesund (78.9°N, 11.9°E), located on the west coast of Svalbard between the Greenland Sea and Barents Sea in the Atlantic sector of the Arctic. Climatologically, this is the warmest part of the Arctic where relatively high tropospheric temperatures are in large part maintained by diabatic heating by the warm ocean (Serreze et al. 2011). At Ny-Ålesund, the Alfred Wegener Institute for Polar and Marine Research operates an atmospheric observatory since more than two decades, comprising measurements from the surface to the upper atmosphere. The Ny-Ålesund surface observations reflect the recent Arctic warming, with an annual mean temperature increase of $+1.3 \pm 0.7$ K per decade in the period 1994 to 2013 (Maturilli et al. 2015). The largest part of this observed warming attributes to the dark winter season, with the December-January-February mean temperature increasing by $+3.1 \pm 2.4$ K per decade (Maturilli et al. 2015). For the same period, the winter LW surface radiation budget is found to increase considerably, with $+11.6 \pm 10.9$ Wm^{-2} for the upward and $+15.6 \pm 11.6$ Wm^{-2} for the downward LW surface radiation (Maturilli et al. 2015). While the upward LW radiation increase is generally linked to the surface temperature increase, the pronounced increase in the downward radiation indicates a radiative contribution from the atmospheric column.

Here, we analyse the daily radiosonde profiles as retrieved in Ny-Ålesund in the period 1993 to 2014 to infer changes in the vertical temperature and humidity profiles over the last two decades. For the detection of such changes, it is mandatory to rely on a consistent dataset. Although the widely used Integrated Global Radiosonde Archive (IGRA) has implemented a formal quality control regarding e.g. formatting problems and physically implausible values (Durre et al. 2006), the archived data originate from different sensors and have changed over time for the various stations, lacking

metadata information. Data are thus globally inhomogeneous but also inhomogeneous over time for the single stations, including the Ny-Ålesund record. It has been recognized that radiosonde measurements developed for weather forecast are subject to hardware and software changes following latest technology, and even procedural changes or reporting practices may have an effect on the data record, introducing problems to the analysis of climate changes (Elliott and Gaffen 1991). Aware of changes in the observation record, we assembled a homogenized Ny-Ålesund radiosonde dataset for the years 1993 to 2014 that accounts for all instrumentally induced errors in the best way known to the current state. The applied corrections to the raw data are described in the next section. The resulting homogenized dataset is provided as supplementary material at <http://doi.pangaea.de/10.1594/PANGAEA.845373> and is the basis for the radiosonde climatology and the analysis of changes in the upper-air atmospheric state over the period 1993 to 2014 in the following sections.

2 Instrumentation and data set

In Ny-Ålesund, the Alfred Wegener Institute conducts radiosonde measurements since 1991. Regular daily 12 UTC launches are operated since November 1992, transferred to the Global Telecommunications System (GTS) via the Norwegian Meteorological Institute under the WMO number 01004. Additional radiosondes have been launched at other daytimes during campaign periods but are excluded from this study to avoid wrong weighting in the statistical analysis. Here, we present the upper-air climatology of the 12 UTC soundings in the period 1993 to 2014 and an analysis of changes that occurred during this period. Numerous studies on climatological trends from long-term radiosonde data records have identified difficulties with inhomogeneity within a single station's data record (e.g. Gaffen 1994; Zhang and Seidel 2011) or among data records from a subset of the global radiosonde stations (Soden and Lanzante 1996; Moradi et al. 2013). Lately, several attempts for radiosonde data homogenization by statistical methods have been developed to overcome discontinuities in the station's radiosonde data record (Lanzante 1996; Gruber and Haimberger 2008; Dai et al. 2011). The inhomogeneity in the historical and active global radiosonde network added to the scientific evidence leading the Global Climate Observing System (GCOS) to initiate the implementation of the GCOS Reference Upper-Air Network (GRUAN), which by now has evolved and provides reference-quality upper-air data products (Bodeker et al. 2016). Ny-Ålesund has been the first radiosonde station certified by GRUAN, and the Ny-Ålesund reference-quality data are available via the GRUAN website. Yet, these data comprise only measurements taken with the Vaisala RS92

radiosonde since 2006. The early Ny-Ålesund radiosonde observations were obtained by the RS80-A radiosonde followed by a 4-year period with Vaisala RS90, which introduced another instrumental discontinuity to the data record. Apart from the changes in radiosonde type, changes in hardware and software have occurred on the receiving side as well. Overall, the standard manufacturer-derived radiosonde product is by no means homogeneous over the described 22-year period. While the knowledge on a large part of the metadata is still available, we attempt to assemble a homogenized radiosonde dataset for Ny-Ålesund based on the best physical correction methods known to the current state by applying well-documented correction algorithms.

In the period 1993 to July 2002 (January 2003), the Vaisala RS80-A radiosonde has been flown on a routine basis. The RS80 A-type HUMICAP humidity measurement is known to have a substantial dry bias especially at low temperatures (Miloshevich et al. 2001). The dominating errors in the RS80-A humidity measurement occur due to temperature dependence as a result of an inaccurate temperature calibration and due to material contamination caused by the storage of the polymer sensor in the sonde packaging material (Wang et al. 2002). In the homogenized Ny-Ålesund data set, the according data have been corrected by applying the correction methods proposed by Wang et al. (2002). Furthermore, the data have been corrected for the time lag that occurs due to the long response time of the humidity sensor at low temperatures by applying the correction algorithm developed by Miloshevich et al. (2004). The figuring of the RS80 humidity sensor allowed the formation of an ice coating on the sensor in liquid water or in ice-supersaturated conditions, sometimes causing the measurements to remain near ice-saturation over large parts of the troposphere, not resembling the conditions of the ambient air. These cases of sensor icing have been excluded from the humidity data in the homogenized dataset. The applied corrections are in line with an earlier publication on the Ny-Ålesund radiosonde humidity observations with focus on ice supersaturation by Treffeisen et al. (2007).

Between 23 July 2002 and 19 May 2006, the daily radiosounding was done with the Vaisala RS90, just like the weekly ozone sounding between 17 November 2002 and 17 January 2007. The RS90 is equipped with two H-type HUMICAP sensors that are heated alternately in order to get rid of condensed water or ice, preventing the effect of sensor icing. Although the H-polymer has a faster sensor response time, time lag is still an issue and is corrected by applying the according time constant in the correction algorithm developed by Miloshevich et al. (2004). As the humidity sensors are not shielded against solar radiation, incoming short-wave radiation can heat the sensors during daytime launches, causing the so-called daytime radiation dry bias. While the effect of nighttime longwave radiation can be neglected, the daytime radiation dry bias needs to be taken into account. At the high

latitude site Ny-Ålesund, the maximum solar elevation is $\sim 30^\circ$. An empirical correction based on data acquired during a campaign in northern Finland during February to August 2009 (Kivi et al. 2009) provides an average correction for polar day conditions.

Finally, after 20 May 2006 (22 January 2007), the daily radiosoundings (weekly ozonesoundings) have been operated with the Vaisala RS92 radiosonde, respectively. Prior to each launch, all RS92 radiosondes were checked with a standard humidity chamber containing saturated air at 100 % relative humidity. The metadata of this additional ground check contributed to the processing of the raw data of all Ny-Ålesund RS92 soundings at the GRUAN Lead Centre with the GRUAN version 2 data processing algorithm. The algorithm applies corrections to the data reducing the dominant errors in temperature and humidity caused by solar radiation, by the time lag of the humidity sensor and by the sensor recalibration during the pre-flight ground-check (Dirksen et al., 2014). In addition, some minor error sources are accounted for, e.g. the removal of temperature spikes caused by the passing of the sensor through the warm wake of the balloon due to the pendulum motion of the payload (Dirksen et al. 2014). The GRUAN processing algorithm, using additional pre-flight ground values, provides reference quality radiosonde profiles with uncertainty for each data point. The RS92 part of the Ny-Ålesund homogenized radiosonde dataset is based on the according GRUAN profiles.

Generally, the applied corrections to the Ny-Ålesund radiosonde data mostly affect the relative humidity values prior to the use of the RS92 radiosonde. Basically, this regards the time period prior to May 2006. As the dry bias correction is largest for measurements in low temperatures (Miloshevich et al. 2001, 2004), the correction effect is largest in the upper troposphere. Indeed, the humidity correction may impact earlier studies using the uncorrected relative humidity values for e.g. cloud microphysical calculations, as the saturation vapour pressure is affected. Regarding studies on the water vapour column, the effect is negligible, since most water vapour is located in the lowermost part of the atmosphere where temperatures are higher and the correction effect is small. In our study, we therefore focus on the specific humidity and integrated water vapour when discussing changes in moisture. In order to homogenize the long-term Ny-Ålesund radiosonde data record, the described extensive corrections from previously published algorithms have been applied to the radiosonde measurements 1993 to 2014. The resulting homogenized radiosonde record is provided as supplementary dataset available at <http://doi.pangaea.de/10.1594/PANGAEA.845373>. The data are interpolated on a regular altitude grid with 50 m vertical resolution in the lower 10 km altitude, and 100 m vertical resolution above, with a maximum altitude of 30 km. As radiosonde temperature and humidity measurements are optimized for 5 m/s ventilation–

condition not given at the surface—surface radiosonde data are not provided. Furthermore, humidity data are not provided above 10 km altitude, as the time-lag error introduces correlated errors in the tropopause region and above that strongly affect the reliability of the measurements in the stratosphere (Dirksen et al. 2014). Wind profiles from radiosondes are derived from tracking the displacement of the sonde from the launch site as a function of time. While for the early RS-80, the radiosonde itself was tracked by receiving OMEGA terrestrial navigational signals with an antenna, Global Positioning System (GPS) satellite signals are used for all radiosondes after September 1997. The positioning signals allow a temporal resolution of a few seconds, but in fact the wind data are filtered to account for the pendulum movement of the radiosondes on a suspension line under the balloon. Radiosonde wind speed on ground is zero by definition, as the radiosonde is not yet displaced. After the balloon acceleration phase just after the launch, the pendulum movement is strongest while the unwinding of the suspension line is still incomplete. The Lagrangian movement of the sonde with the wind field may thus be assumed not earlier than half a minute after the launch, therefore wind data are provided from 200 m altitude in the homogenized Ny-Ålesund radiosonde dataset.

While the supplementary dataset contains all radiosondes launched in Ny-Ålesund, the following analysis is based exclusively on the 12 UTC profiles.

3 Upper-air climatology

From the corrected, homogenized 22-year Ny-Ålesund radiosonde dataset, an upper-air climatology is presented for the vertical profiles up to 30 km altitude. While climatologies based on observational data are available for surface and ground-based parameters, this is the first upper-air climatology from radiosonde measurements for a high European Arctic station. As the launch site Ny-Ålesund is located close to the coastline of a fjord surrounded by mountains, orographic effects on the vertical atmospheric structure are expected. The local imprint on the general flow emerges from the combination of the vertical wind profiles.

3.1 Wind

The orography around Ny-Ålesund has a strong influence on the air flow in the lowermost kilometre of the atmosphere (Beine et al. 2001; Esau and Ripina 2012). Ny-Ålesund is located at the coast of the northwest-southeast-oriented Kongsfjord that is surrounded by mountains with typical altitudes up to 800 m. The given topography causes a channelling of the flow in this part of the atmosphere in alignment with the

valley axis, resulting in a distinct southeast main wind direction throughout all seasons (Fig. 1). Less frequent is the channelling in the opposite direction, with north-westerly flow in the lowermost kilometre being observed primarily during spring and summer. Above the topographic imprint, the free troposphere is characterized by a general westerly flow.

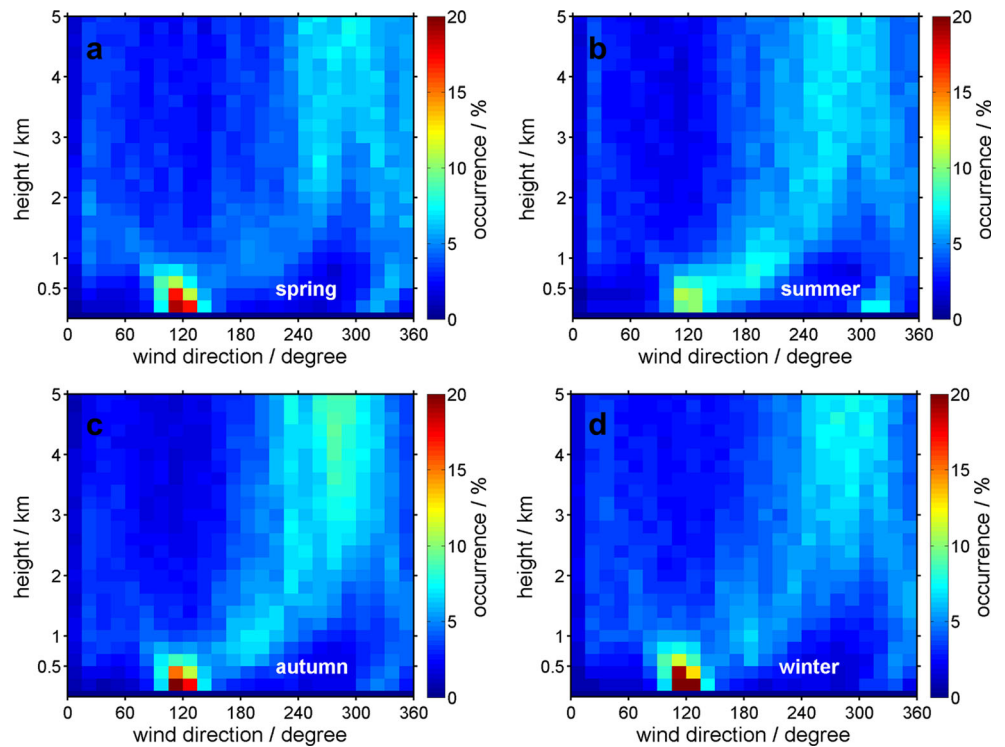
The vertical distribution of wind speed is illustrated for the different seasons in Fig. 2. In the troposphere, wind speeds up to 15 m/s are common, while they rarely exceed 20 m/s. Visible in all seasons, although not observed very frequently above Ny-Ålesund, is the tropopause jet with high wind speeds up to 50 m/s. In the stratosphere above, the large seasonal differences in flow strength and direction become apparent. The stratospheric summer circulation with easterly winds above 20 km (Fig. 3) is characterized by low wind speed below 10 m/s. The dynamic situation changes dramatically with the formation of the polar vortex in the autumn season September–October–November, with stronger stratospheric winds from westerly directions (Figs. 2 and 3). The presence of the polar vortex is also visible in the winter season December–January–February, but both wind direction and speed are more variable and thus appear smeared. The variability is related to the dynamics of the stratospheric polar vortex moving across the Arctic due to planetary wave interaction. While in springtime, the onset of the easterly zonal circulation is already observed above 25 km, and the remnants of the polar vortex with strong westerly winds are still active below.

As radiosonde data are frequently used for satellite validation or in comparison with model studies, the geographic position of the measurement has to be considered. Balloon drift can have a substantial impact on the measurement location compared to the launch location. Therefore, the geographic position is provided for each sounding on all vertical levels in the homogenized dataset, and an overview of the sounding's footprint is provided in a plot for each year in the supplementary data.

3.2 Temperature

The seasonal mean state of temperature above Ny-Ålesund for spring (March, April, May; MAM), summer (June, July, August; JJA), autumn (September, October, November; SON) and winter (December, January, February; DJF) as detected by radiosondes in the period 1993 to 2014 is shown in Fig. 4, respectively. In the troposphere, the temperature distribution of the different seasons resembles in their structure, being different only in absolute quantity. In contrast, the stratospheric part of the temperature profile gives a more diverse picture. From the standard deviation and the minimum and maximum temperature lines, obviously summer is the season with the lowest interannual variability. The tropopause structure is clearly visible in the summer months, while the

Fig. 1 Occurrence frequency of wind direction from radiosonde profiles 1993–2014 counted in 15-degree bins for each height step, separated to seasons as spring (a), summer (b), autumn (c) and winter (d)



stratosphere above becomes almost isothermal to about 30 km altitude. The anticyclonic circulation in the Arctic stratosphere collapses annually in late August (Hare 1960). Cooling of the middle stratosphere begins early in that month, and the cooling wave spreads rapidly downwards. With the change

in stratospheric circulation, the variability of temperature profiles gets larger during the autumn season. Stratospheric temperatures are lower, with a negative temperature gradient above the tropopause region since radiative heating by solar radiation vanishes. The formation of the stratospheric polar

Fig. 2 Occurrence frequency of wind speed from radiosonde profiles 1993–2014 counted in 1-m/s bins for each height step, separated to seasons as spring (a), summer (b), autumn (c) and winter (d)

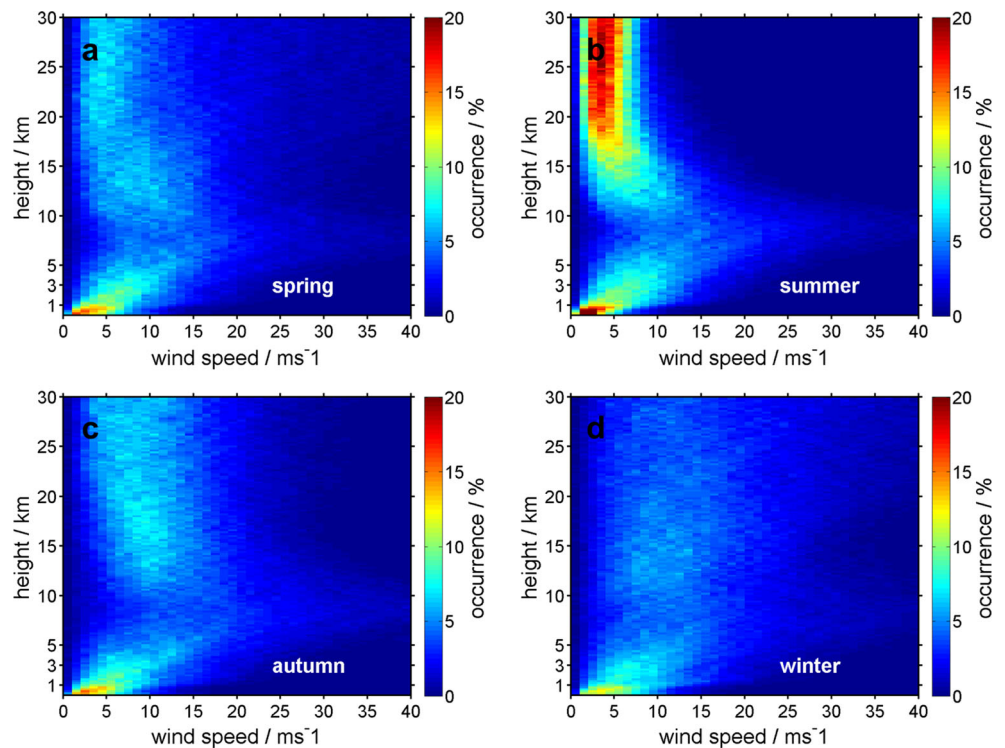
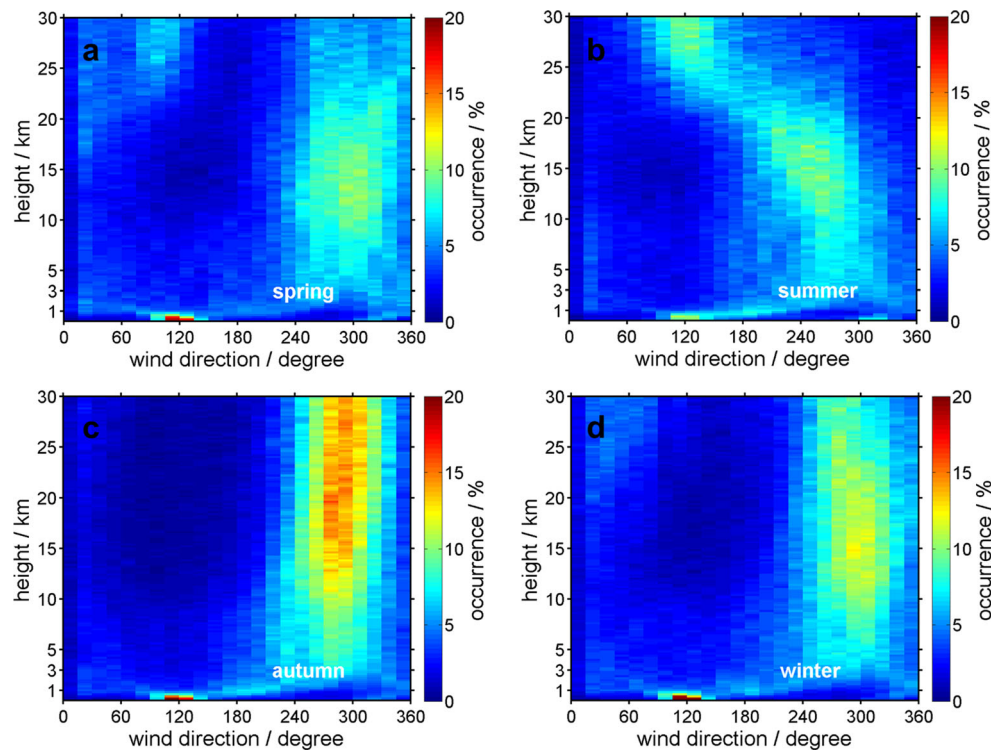


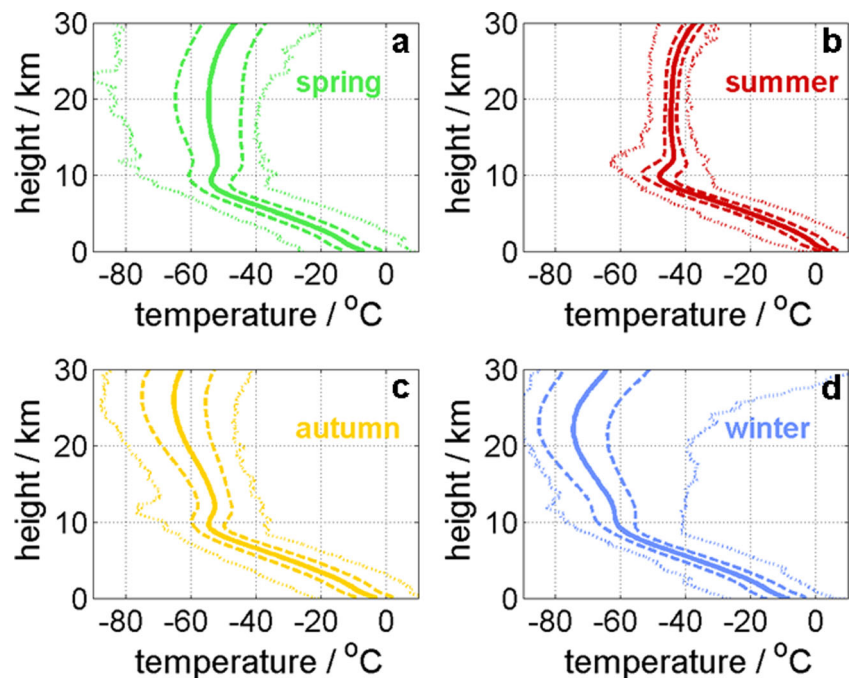
Fig. 3 Occurrence frequency of wind direction from radiosonde profiles 1993–2014 up to 30 km counted in 15-degree bins for each height step, separated to seasons as spring (a), summer (b), autumn (c) and winter (d)



vortex with its cold pool introduces a large variability in stratospheric temperatures when looking at a single Arctic station. The Arctic polar vortex is characterized by its frequent displacement from the pole due to wave interaction-related dynamics, including vortex break-up episodes. In Ny-Ålesund, the influence of the stratospheric polar vortex is

certainly strongest in the winter season, with low stratospheric temperatures allowing the formation of polar stratospheric clouds (Maturilli et al. 2005; Massoli et al. 2006). On the other hand, sudden stratospheric warming events (Scherhag 1952) can warm the lower stratosphere to considerably high temperatures, even exceeding the surface temperature. The spring

Fig. 4 Seasonal mean temperature profiles from Ny-Ålesund radiosonde profiles 1993 to 2014, indicating ± 1 standard deviation (dashed lines) as well as minimum and maximum temperatures (dotted lines) occurring during this 22-year period



season is on average much warmer in the stratosphere, with a slightly positive temperature gradient above 20 km. Yet, the broad standard deviation indicates a large variability of stratospheric temperature in spring, and the minimum temperature can differ by about -20 K from the average. These low stratospheric temperatures are seen in early springtime during some years, when the stratospheric polar vortex is persistent and the vortex cold pool located above Svalbard.

Generally, the vertical temperature gradient defines the separation between the vertically mixed troposphere and the stably stratified stratosphere, known as the thermal tropopause. While the temperature gradient in the upper troposphere follows the adiabatic temperature gradient, the temperature distribution in the stratosphere is less affected by vertical dynamic processes due to its stable stratification and is mainly controlled by radiative processes. During the sun-lit period, the thermal tropopause is a distinct feature in the Ny-Ålesund temperature profiles. Yet, radiative cooling in the absence of solar radiation during polar night and the dynamics of the polar vortex affect the temperature distribution in the upper troposphere/lower stratosphere (UTLS) region. As a result, the thermal tropopause above Ny-Ålesund is frequently indistinct during the winter months as shown in the example of 29 December 2012 presented in Fig. 5, primarily due to a too low static stability in the lower stratosphere. Here, the WMO definition of the thermal tropopause being the lowest level at which the lapse rate decreases to 2 K/km or less, while the average lapse rate from this level to any level within the next higher 2 km does not exceed 2 K/km (WMO 1957), does not allow to identify a thermal tropopause. In fact, it depends on synoptic scale conditions whether

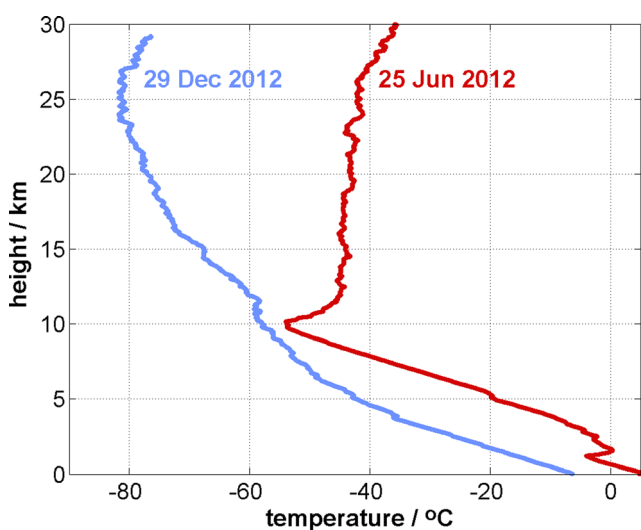


Fig. 5 Temperature profiles measured by radiosonde from Ny-Ålesund on 29 December 2012 (blue line) and on 25 June 2012 (red line), respectively

the thermal criterion yields a meaningful tropopause or not, and the thermal criterion has been found to be inappropriate for polar winter (Zängl and Hoinka 2001). Alternative tropopause definitions based on potential vorticity threshold values or on vertical gradients in conserved trace gases are not applicable to the available radiosonde parameters; therefore, tropopause height is not explicitly provided in the dataset.

The annual cycle of the monthly mean tropospheric temperature profiles is shown in Fig. 6, clearly illustrating the imprint of polar day and polar night conditions in the warm and cold half of the year. Maximum temperatures occur during summer with approximately 5 °C close to the surface, -20 °C in 5 km and -50 °C around 9 km, while the temperature minimum occurs during winter with -15 °C close the surface, -35 °C in 5 km and roughly -60 °C in the upper troposphere. Obviously, averaging over the 22-year period blurs out smaller-scale temporal and spatial structures. Very frequently observed are temperature inversions in the lower troposphere, as e.g. in the temperature profile on 25 June 2012 shown in Fig. 5. Thermal inversion layers are areas where temperature is increasing with altitude, preventing air from rising and thus acting as a cap for the colder air below the inversion. They occur when a warm, less dense air mass moves over a dense, cold air mass. On the basis of the homogenized radiosonde dataset with the lowest data point at 50 m altitude, it is not possible to explicitly distinguish between elevated or surface-based inversions. For studies focusing on the near-surface temperature distribution and the planetary boundary layer structure, the combination with tower measurements close to the launch site are an option (e.g. Maturilli et al. 2013). From the homogenized radiosonde data, the annual frequency distribution of thermal inversion layers in the lower troposphere occurs as

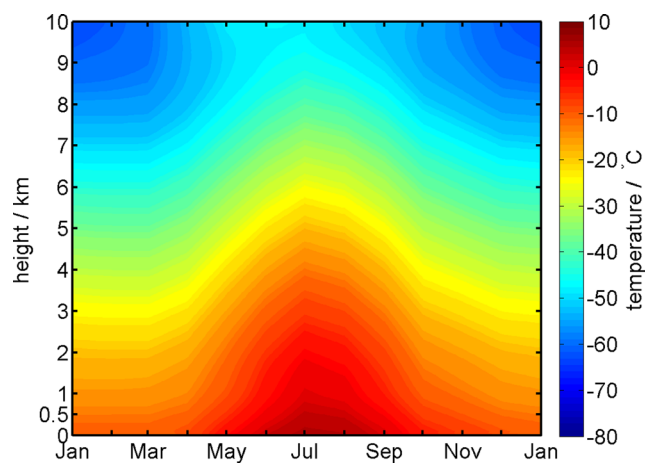


Fig. 6 Annual cycle of tropospheric temperature above Ny-Ålesund from radiosonde observations 1993 to 2014

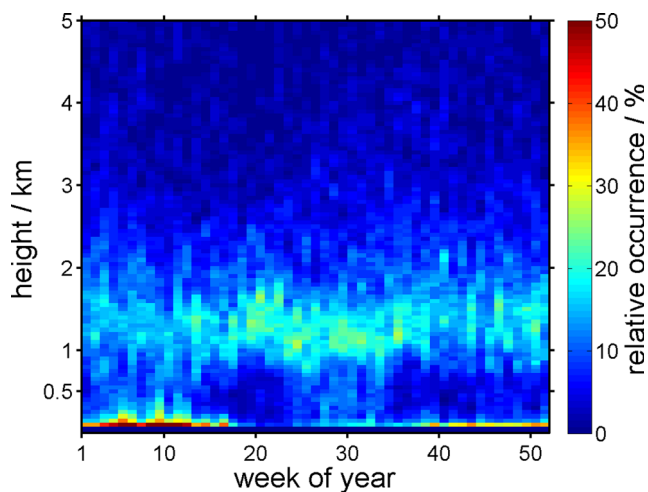


Fig. 7 Relative occurrence frequency of temperature negative-lapse rate layers in weekly slots of all soundings in the period 1993–2014

shown in Fig. 7. The analysis is based on all observed negative-lapse rate layers, as commonly more than one inversion layer is detected in an individual temperature profile. The minimum depth of the negative-lapse rate layers requires 100 m, similar to other studies that rather focus on inversion top or base height and on inversion strength (e.g. Kahl 1990; Vihma et al. 2011).

Several processes may contribute to the formation of the thermal inversion layers, some of them related to the local orography. In the mountainous landscape, up drift and descending flow are common features in the Svalbard fjords that can trigger the formation of thermal inversions by cold air flow from the mountain peaks and glaciers sliding under the warmer air rising from the valley. In addition, thermal inversions can form in areas with significant snow cover since the snow surface radiatively cools the air near the ground. This radiative surface cooling is expected to be less important during the summer months in Ny-Ålesund, when the lower altitude fjord landscape is snow-free. In fact, Fig. 7 shows a spatiotemporal maximum in thermal inversion occurrence frequency in the lowermost 500 m during the winter and spring season. These low inversions are likely connected to surface-atmosphere interaction processes and the stabilization of the atmosphere by radiative cooling. In the higher altitude range between 1 and 2 km, a second maximum in thermal inversion occurrence frequency emerges. This higher inversion layer appears throughout the year and is present in up to 56 % of all soundings. It is situated above the altitude range of the local orographic wind channelling (Fig. 1) and thus is a feature that presumably is not limited to the inner Kongsfjord area, but applies to the Svalbard fjord landscape in general. In fact, earlier studies by tethered balloon in different Svalbard fjords showed that

warm air advection by the synoptic scale flow in the free troposphere generates the occurrence of elevated thermal inversions (Vihma et al., 2011). As advected warm air masses meet the mountain or glacier tops and mix with the katabatic flow, the introduced increase in temperature supports the lift of the flow above the cold air pool in the valley. Generally, temperature inversions affect the degree of coupling of the atmospheric boundary layer to the free troposphere and thus have an impact on a broader scale. Furthermore, thermal inversions often relate to the existence of a stratiform cloud deck (Sedlar and Tjernström 2009). In the fjord valley, the mixed layer is characterized by wind blowing over the water surface mixing moist surface air upwards. Radiative cooling of moist air affects the temperature distribution, and stratiform clouds are formed once the condensation level is reached but remain capped below the temperature inversion. In this context, the distribution of atmospheric humidity is a key component.

3.3 Humidity

Relative humidity (RH) is the measured quantity that is mostly affected by the corrections applied to the data set in order to homogenize the long-term radiosonde data record. From the corrected data, the annual cycle of tropospheric relative humidity above Ny-Ålesund is shown in Fig. 8, with a clear maximum during the warmer summer months. Referring to the relative humidity with respect to water, RH is highest in the lower part of the troposphere, implying high probability for liquid cloud occurrence in the lower 2 km of the atmosphere. Considering the low temperatures of the upper troposphere, relative humidity with respect to ice (not shown) reveals a second maximum in the upper troposphere,

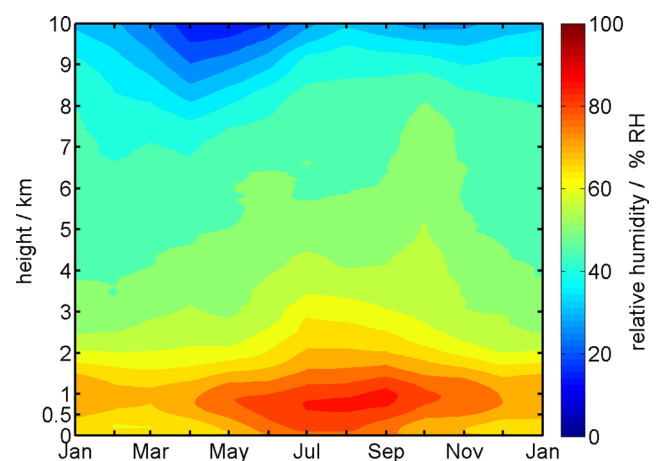


Fig. 8 Annual cycle of relative humidity (with respect to water) above Ny-Ålesund from radiosonde observations 1993 to 2014

accounting for the occurrence of ice clouds. In the Ny-Ålesund radiosonde data, ice supersaturation occurs mostly in a broad band between 6 and 9 km in winter, shifting towards higher altitudes in summer (Treffeisen et al. 2007). In terms of cloud radiative forcing, low-level liquid and mixed-phase clouds are the most important contributors to the Arctic surface radiation balance, while ice clouds have only a small radiative impact (Shupe and Intrieri 2004). Here, rather than discussing relative humidity in the context of cloud microphysics, we aim to emphasize on the importance of water vapour as a greenhouse gas. For further analysis, relative humidity is therefore converted to specific humidity applying the saturation vapour pressure equation by Hyland and Wexler (1983), resulting in the annual cycle shown in Fig. 9.

The annual distribution of specific humidity follows the annual cycle in temperature (Fig. 6), with the highest moisture content occurring during the warm summer months. In absolute quantities, most water vapour is found in the lowermost 2 km of the atmosphere. Thus, when considering integrated water vapour, the major column contribution originates from this low part of the humidity profiles. It is also the altitude range where humidity inversions are observed in the Arctic (Nygård et al. 2014). Since the specific humidity is commonly decreasing with altitude (Fig. 9), layers of increasing specific humidity with altitude are consequently defined as humidity inversions. The relative occurrence frequency of humidity inversion layers is shown in Fig. 10, similar to the thermal inversion layers in Fig. 7. Overall, humidity inversions occur more frequently than temperature inversions, and rather located in the altitude range just below the elevated temperature inversions.

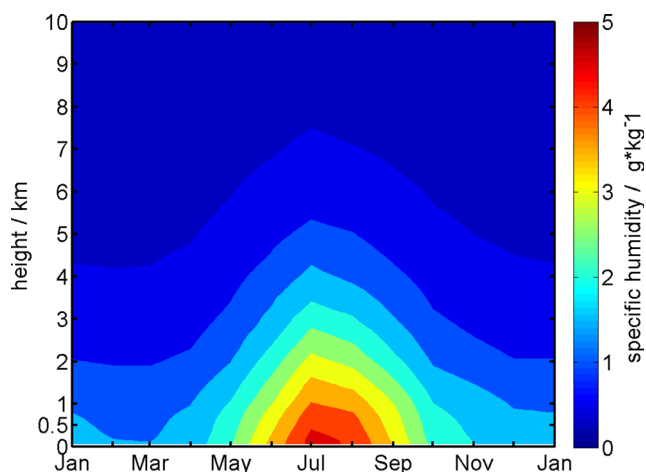


Fig. 9 Annual cycle of specific humidity above Ny-Ålesund from radiosonde observations 1993 to 2014 applying the vapour pressure formula by Hyland and Wexler (1983)

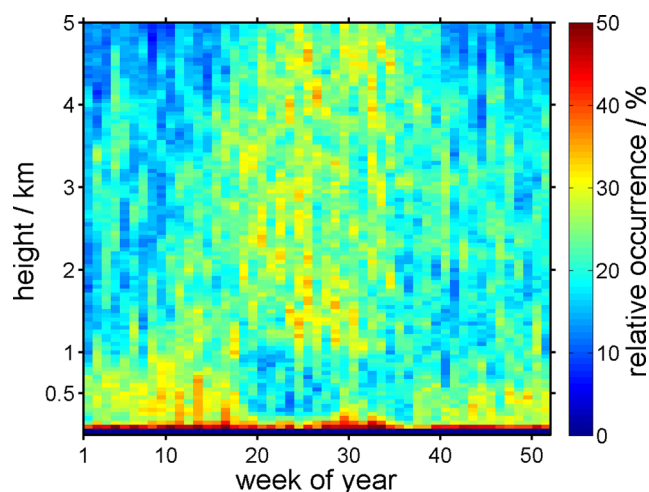


Fig. 10 Relative occurrence frequency of specific humidity inversion layers in weekly slots of all soundings in the period 1993–2014

Throughout the whole year, humidity inversions are frequently observed below 200 m altitude. Still, other studies suggest that these low humidity inversions are rather not surface-based, as Vihma et al. (2011) found surface-specific humidity exceeding the air-specific humidity in the majority of tethered balloon measurements from Ny-Ålesund, and Nygård et al. (2014) even found 80 % of Arctic humidity inversions being elevated from the surface. Above 200 m up to about 1 km altitude, a clear seasonality in the occurrence of humidity inversions becomes apparent (Fig. 10). In winter and spring, humidity inversion occurrence above Ny-Ålesund is much higher in this altitude range than during the summer or autumn season. Highest (lowest) frequency of occurrence of humidity inversions in winter (summer) has also been found in other Arctic radiosonde and Atmospheric Infrared Sounder (AIRS) data (Devasthale et al. 2011). The apparent high occurrence frequency of humidity inversions in the free troposphere in summer is due to the relatively high absolute water vapour quantities facilitating the fulfilment of the inversion criteria.

Generally, multiple humidity inversions may occur in a single profile as is also valid for the temperature inversions. However, as the relative occurrence frequency of temperature and humidity inversions indicate (Figs. 7 and 10, respectively), negative temperature lapse rate and increasing water vapour with height have no strong temporal or spatial dependence. While in 84 % (62 %) of all profiles a humidity inversion is detected below 2 km (between 0.8 and 2 km), temperature inversions are found in 75 % (56 %) of the profiles, respectively. Considering all Ny-Ålesund radiosonde profiles, the significant correlation between temperature and humidity inversions below 2 km is only $r = 0.22$, being slightly higher ($r = 0.24$) when considering only the winter season. The observed humidity inversions should therefore not be

considered as a side effect of the temperature inversions, as they occur in independent vertical layers.

4 Upper-air trend estimates

Over the last two decades in Ny-Ålesund, surface warming and changes in the surface radiation balance components have been detected (Maturilli et al. 2013, 2015). Here, we analyse related changes in the upper-air profiles measured by radiosondes in the period 1993 to 2014. Though there may still remain an uncertainty associated with the difficulties of radiosonde humidity measurements below -40 °C despite the applied corrections to the long-term data record, we are confident that the detection of substantial changes in the atmospheric humidity below 3 km altitude is reliable. Essentially, the vertical profiles of the homogenized radiosonde dataset allow determining a change in moisture content in the atmospheric column. Indeed, the integrated water vapour (IWV) calculated from the Ny-Ålesund radiosonde humidity measurements indicates an increase in atmospheric moisture over the years (Fig. 11). If the radiosonde data were used without the applied corrections for the dataset homogenization, the increase would have been even larger due to the dry bias of the earlier radiosonde products. Considering the IWV annual mean from the homogenized Ny-Ålesund radiosonde dataset, the increase of $+0.11 \pm 0.96$ kg/m² per decade is negligible, but when considering the IWV winter mean, the observed increase of $+0.83 \pm 1.22$ kg/m² per decade is quite substantial for the winter season. Though small in absolute quantities, the seasonal increase in IWV during the winter

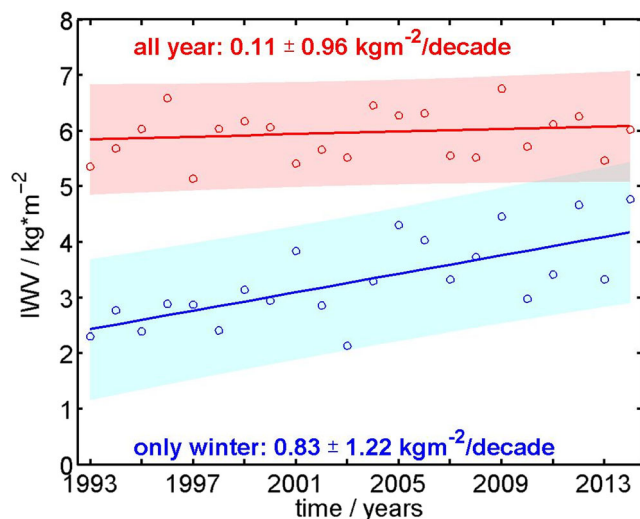


Fig. 11 Integrated water vapour (IWV) from radiosonde measurements for the annual mean (red circles) and the winter season mean (blue circles). The increase over the period 1993 to 2014 is given by the linear regression (coloured lines) ± 1 standard deviation (colour shaded), respectively

months is much more rapid, indicating that atmospheric humidity may well contribute to the observed winter increase in longwave downward radiation. Although IWV refers to the entire atmospheric column, the largest contribution is given by the lowest 2 km of the profile where most water vapour is found (see Fig. 9). An advantage of radiosonde measurements is their high vertical resolution, allowing the identification of specific humidity inversion layers. As the occurrence of humidity inversions is common in the Ny-Ålesund snow-covered seasons, a change in humidity inversion properties regarding their frequency, altitude, strength or depth, could potentially be the cause for the observed moisture increase.

To distinguish the moisture contribution of the humidity inversions from the larger-scale background humidity profile, the quantity of specific humidity in the inversion layers has been extracted from the profiles as shown in Fig. 12. For each specific humidity profile, the base and top of each humidity inversion layer exceeding 100 m vertical extent have been identified to crop a background humidity profile that excludes the humidity contribution of the humidity inversion layers. The amount of specific humidity has then been integrated separately for the inversion contributions and the background profiles, respectively.

The inversion layer contribution and the background profile contribution to the integrated specific humidity are shown in comparison to the total column for each season in Fig. 13, respectively. The absolute quantities vary in seasonal dependence, the summer months being much more humid than the winter months. Generally,

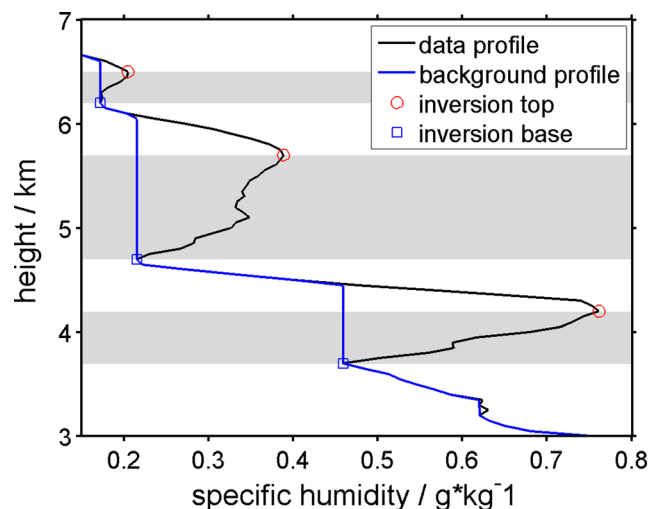
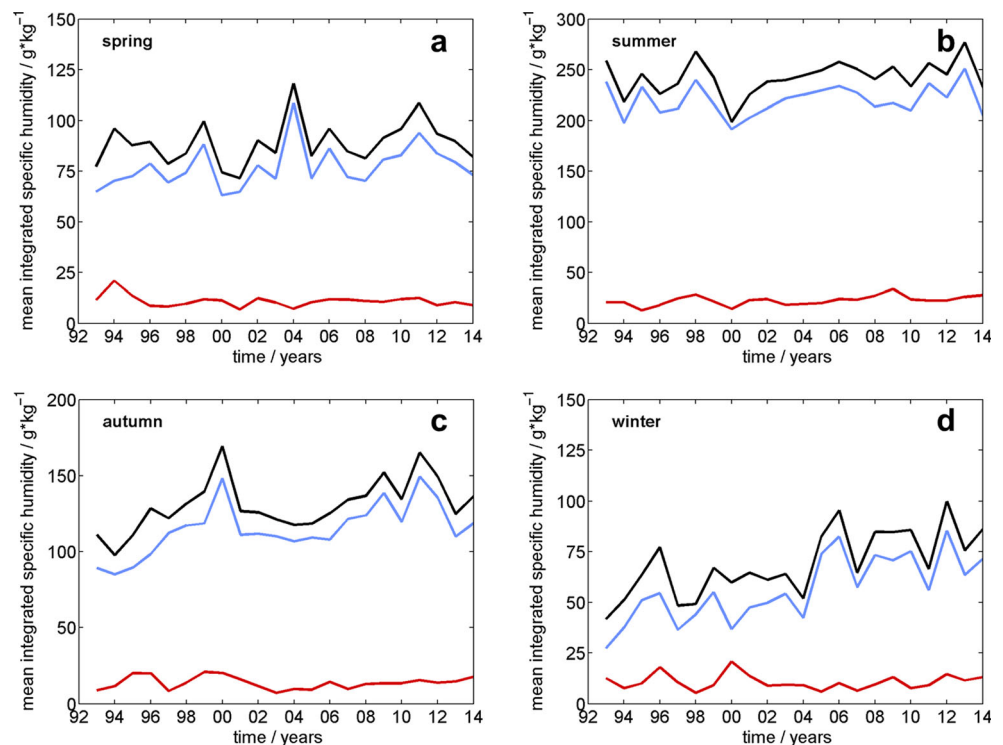


Fig. 12 Sample specific humidity profile from radiosonde measurements (black line), with base (blue circle) and top (red circle) of several humidity inversions. Inversion layers are considered where specific humidity increases with height (grey shading), while the background humidity profile (blue line) cuts off the inversion layer from the inversion base until the same value is the same background value is reached above the inversion top

Fig. 13 Integrated specific humidity of the total profiles (black lines), the background humidity profiles (blue lines) and the inversion layers (red lines), in mean values for the different seasons: spring (a), summer (b), autumn (c) and winter (d)



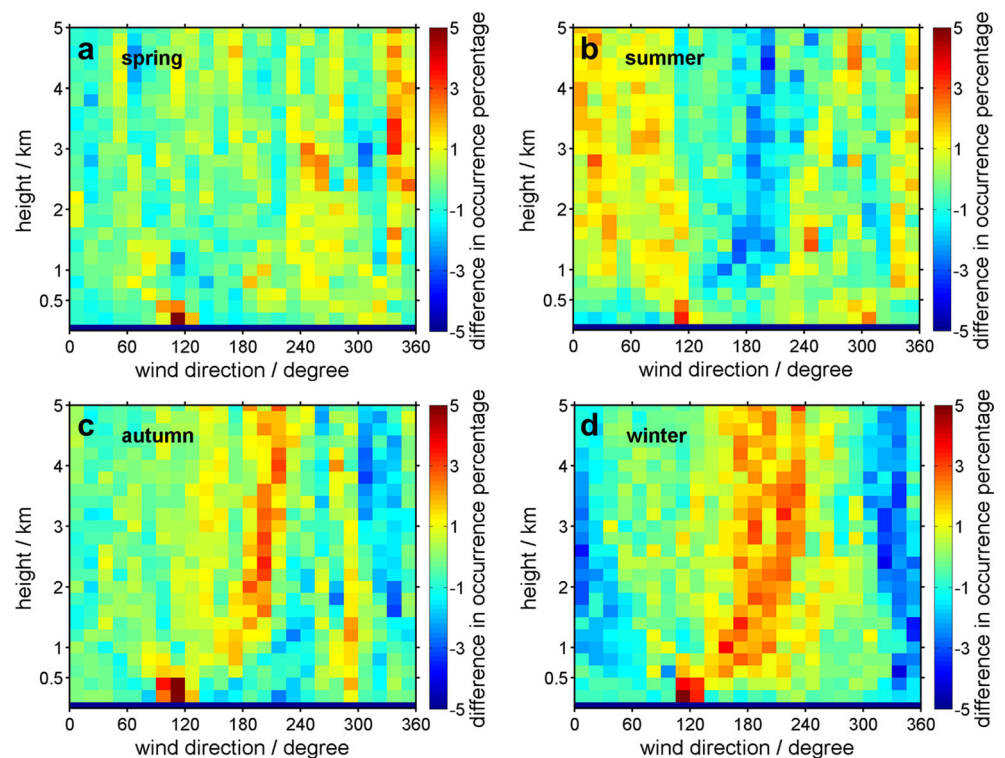
the relative contribution of the humidity inversion layers to the total column is in the order of 10 % for all seasons but winter, when the absolute values of the integrated specific humidity are smallest and the occurrence frequency of humidity inversions in the lowermost atmosphere is highest. More importantly, the contribution of the humidity inversions remains stable over the years. Considering the IWV increase in winter season, it turns out that it is not related to a change in humidity inversion occurrence. Local mesoscale effects on the structure of the humidity profiles can thus be excluded to cause the observed IWV increase. Instead, we find indeed that the moisture increase in the large-scale background humidity profile (Fig. 13) is responsible for the increasing moisture content in the atmospheric column above Ny-Ålesund in winter.

In this context, several processes need to be discussed as sources of the observed humidity increase. Potentially, the decreasing sea ice cover of the Arctic Ocean North of Svalbard provides large areas with intensified evaporation and latent heat exchange to the Arctic atmosphere, especially during the period of sea ice minimum in autumn (Fig. 14). Warm anomalies have been found in Atlantic water on the way to the Arctic Ocean, with the West Spitsbergen Current carrying the warm, saline Atlantic water north above the shelf slope west of Svalbard (Beszczynska-Möller et al. 2012), being a potential regional source for higher atmospheric humidity due to increased evaporation.

Additionally, changes in the atmospheric circulation enhancing the advection of warm and moist air from lower latitudes have to be considered.

Regarding the warming of the atmospheric column, Fig. 15 shows the temperature change per decade as retrieved from the linear regression of the monthly mean temperature profiles. Only those parts where the regression uncertainty is smaller than the regression coefficient are considered statistically significant. Over the 22-year period of the homogenized radiosonde data record, changes in the vertical temperature distribution are found throughout the free troposphere with large diversity for the different seasons, but only the tropospheric warming in January and February is statistically significant from the surface to 7700 m and to 8650 m, respectively. The two winter months are characterized by a strong temperature increase reaching about 3 K per decade in the free troposphere, with maximum values higher than 3.6 K per decade in the boundary layer below 1 km, being highest the closer to the surface. Due to statistical insignificance, no quantitative conclusions can be drawn for the other months. Yet qualitatively, it appears that the magnitude of temperature change differs between the boundary layer below 1 km and the free troposphere above. It seems that local conditions within the lowermost kilometre of the atmosphere affect the vertical temperature distribution of the Ny-Ålesund boundary layer. Yet, while local boundary processes may amplify the general warming in the

Fig. 14 Difference in the relative occurrence frequency of wind directions, retrieved by subtracting the early period [1993 to 2003] from the late period [2004 to 2014] of the homogenized Ny-Ålesund radiosonde dataset, separated for the different seasons spring (a), summer (b), autumn (c) and winter (d)



lowest part of the profiles, they are excluded to be the cause for the observed warming of the above decoupled free troposphere. Potentially involved processes affecting the additional warming in the boundary layer are related to e.g. the presence of the capping inversion, the occurrence of low-level clouds, or changes in surface fluxes. Also, moist intrusions from lower latitudes were found to result in a bottom-amplified warming (Woods and Caballero 2016).]

Furthermore, from the radiosonde wind data, it is found that frequency of occurrence of fjord-axis wind channelling below 500 m has increased throughout all seasons. The enhanced directional decoupling from the free tropospheric flow is accompanied by smaller wind velocities. While the tropospheric wind speed above 1 km does not show any relevant changes, the occurrence frequency of small wind velocities below 5 m/s in the lowermost kilometre has decreased in the last decade, being substituted by almost windless conditions. The smaller wind velocities of the channelled flow imply less ventilation within the boundary layer with cold air from the glaciers. Potentially, this reduced cold air advection also contributes to the observed stronger warming in this lowermost part of the atmosphere.

Based on the 22-year homogenized radiosonde dataset, an attempt to visualize changes in the atmospheric flow reaching the troposphere above Ny-Ålesund is shown in Fig. 14. Here, the difference between the earlier and the more recent period is illustrated by subtracting the occurrence frequency of the different

wind directions for period 1993 to 2003 from period 2004 to 2014. While for the spring season, changes in wind direction occurrence appear scattered with no clear pattern, it seems that in the summer period the large-scale atmospheric flow above 1 km arrives less frequent from the south and consequently more frequent from other directions. The picture changes with the season of autumn, when the large-scale tropospheric flow occurs more from southerly directions and less from north/

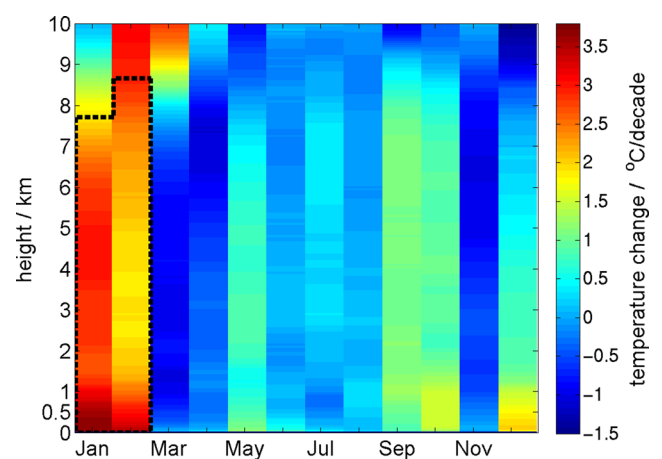


Fig. 15 The monthly temperature change over the period 1993 to 2014 for each 50 m altitude level, retrieved from the linear regression of the monthly mean temperature profiles. Statistical significance is given where the regression uncertainty is smaller than the regression coefficient, a condition met only in January and February (marked by dashed black line)

northeast. Most prominent are the changes in the tropospheric wind regime above Ny-Ålesund during winter season, when the large-scale flow is much more frequent from south-southeast in the later period compared to the earlier years. At the same time, wind from northerly directions is less frequent to the same amount. The difference in observed wind directions implies that changes in large-scale atmospheric transport impact the atmospheric column above Ny-Ålesund during the winter season. With the observed increase of wind from the south, it is plausible that the advection of warm and moist air from lower latitudes is the reason for the observed large-scale temperature and humidity increase.

5 Atmospheric circulation changes

From the observed changes in the Ny-Ålesund upper-air measurements, it appears as if the strong winter increase in tropospheric temperatures and water vapour column is related to changes in the synoptic flow across the Svalbard archipelago, advecting warm and moist air from the south. On the other hand, vertical wind profiles indicate an increase of synoptic flow from the north during the summer months. Such changes in atmospheric circulation in the Svalbard region have to be linked to a changing pattern of synoptic systems. Figure 16 shows the difference in mean sea level pressure between the early period (1993–2003) and the later period (2004–2014) from ERA-interim reanalyses monthly means, for winter (DJF) and summer (JJA).

It turns out that during the winter months 2004–2014, a high pressure anomaly indicates a shift of the centre of the Siberian high towards the west or a more frequent occurrence of a Scandinavian blocking high. A high pressure anomaly was located over the eastern Arctic ocean, including Svalbard, Northern Scandinavia

and Siberia, with a maximum southeast of Svalbard (Fig. 16a). For the summer months, a high pressure anomaly is located over the western Arctic, to the north and west of Svalbard, largely covering the North Pole and Greenland (Fig. 16b). From the Ny-Ålesund viewpoint, these pressure anomalies contribute to anticyclonic advection from the south during winter and anticyclonic advection from the north during summer, confirming the radiosonde wind direction analysis.

The leading variability pattern of the sea level pressure field is the Arctic Oscillation (e.g. Thompson and Wallace 1998). Here, we analyse the AO during the early period 1993–2003 and the late period 2004–2014 similar to the radiosonde dataset.

From the ERA-interim monthly mean sea level pressure data poleward of 20°N for 1993 to 2014, the AO patterns have been calculated as the leading empirical orthogonal function (EOF) (e.g. Preisendorfer 1988; Hannachi et al. 2007) both for the winter season (DJF) and the summer season (JJA). On this basis, the daily AO indices were obtained by projecting the daily mean sea-level pressure anomalies poleward of 20°N onto the winter and summer AO patterns, respectively. The short time period with large variability does not allow for the retrieval of a trend. Yet, when dividing into early and late periods (1993–2003 and 2004–2014, respectively), differences in the frequency of occurrence of positive and negative AO indices become evident. Both during the summer and the winter seasons, there has been a shift from more positive anomalies 1993–2003 towards more negative anomalies 2004–2014 (Fig. 17).

Generally, the positive AO pattern is characterized by a strong Icelandic low pressure system and a strong high pressure system over the Azores, inducing an increased westerly flow with little meridional transport over the North Atlantic. As we find a shift towards

Fig. 16 Difference in mean sea-level pressure between periods 1993–2003 and 2004–2014, for winter months December–January–February (a) and summer months June–July–August (b), from ERA-interim reanalyses

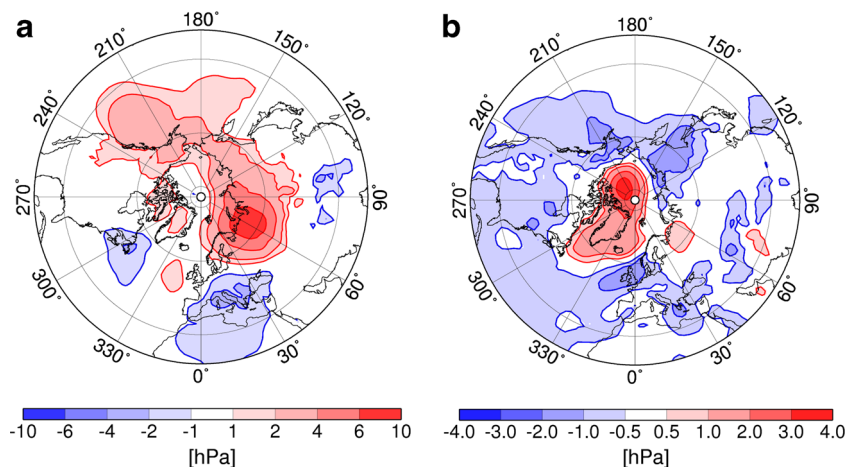
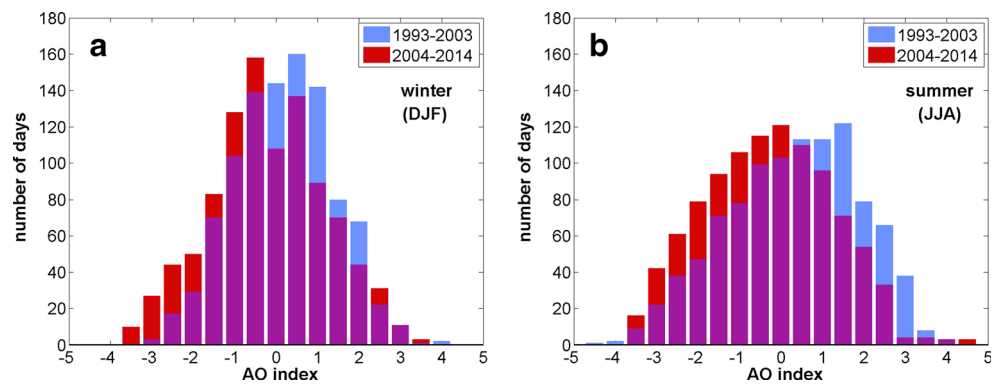


Fig. 17 Daily AO indices for the winter months December–January–February (a) and the summer months June–July–August (b), divided into the early period 1993–2003 (blue) and the late period 2004–2014 (red; overlap in purple), respectively



negative anomalies of this pattern, more frequent blocking high situations are expected, reducing the westerly flow and allowing for increased meridional transport.

We therefore conclude that the observed warming and moistening of the tropospheric column above Ny-Ålesund is to large parts related to the changes in the atmospheric circulation patterns.

6 Conclusions

For more than 22 years, radiosonde measurements have been operated in Ny-Ålesund, Svalbard. Aware of the instrumentation discontinuities in the data record, the manufacturer-provided vertical profiles have been corrected by applying well-documented correction algorithms. The resulting homogenized radiosonde dataset is given with 50 m (100 m) vertical resolution below (above) 10 km, respectively, up to an altitude of 30 km. It is published (<http://doi.pangaea.de/10.1594/PANGAEA.845373>) as a suitable dataset for e.g. the evaluation of climate model studies or satellite observations. The presented climatology from the 1993 to 2014 radiosonde data provides an overview of the general climatic distribution of temperature, humidity and wind in the vertical column above Ny-Ålesund and is a valuable background for atmospheric process studies on smaller scales.

While the annual cycle of tropospheric temperature and humidity has a smooth distribution with maxima in the lower atmosphere in summer, the single profiles frequently record the presence of one or more inversion layers. In fact, temperature and humidity inversions below 2 km altitude are detected in 75 and 84 % of all soundings, respectively. Very low temperature inversions prevalently observed during the snow-covered dark season are presumably radiative surface-based inversions. Throughout the year, the occurrence of a capping inversion around 1 km is common, as detected between 0.8 and 2 km in 56 % of all soundings. This capping inversion contributes to the decoupling of the boundary layer from the free troposphere that is facilitated by the fjord axis channelling of the wind below 800 m caused by local orography.

The boundary layer is also the altitude range where the occurrence of specific humidity inversions has its maximum. While humidity inversions below 200 m are found frequently throughout the whole year, they are observed in the broader boundary layer up to 1 km predominantly in winter and in the snow-covered season. The significant correlation between temperature and humidity inversions below 2 km is only $r = 0.22$, corresponding to their general occurrence in independent vertical layers and the more frequent detection of humidity inversions. Since 70–90 % of the downward longwave radiation to the surface is emitted from the lowermost 1 km of the atmosphere (Ohmura 2001), Devasthale et al. (2011) concluded that humidity inversions have potentially significant impact on the radiative characteristics of the atmosphere.

On the background of increasing surface downward longwave radiation in Ny-Ålesund (Maturilli et al. 2015), the contribution of humidity inversions to the total integrated water vapour (IWV) has been analysed for the period 1993 to 2014. It turns out that the contribution by humidity inversions remains stable over the years, while for the winter months an increase is found in the total IWV, identified to be caused by a moisture increase in the large-scale background humidity profile.

Large-scale processes are also responsible for the significant warming of the atmospheric column detected in January and February. For these winter months, the temperature increase is found to reach up to about 3 K per decade throughout the free troposphere, being even stronger up to 3.6 K per decade in the boundary layer below 1 km altitude. The changing temperature in the winter troposphere above Ny-Ålesund is related to a change in wind direction observed during the same period 1993 to 2014. Compared to the earlier period 1993 to 2003, the wind direction in the later period 2004 to 2014 has occurred much less frequent from north-westerly directions and to the same amount much more frequent from southern directions in the free troposphere in winter. Synoptic flow from the south towards the Svalbard region implies the advection of warm and humid air from lower latitudes. Effectively, the Ny-Ålesund radiosonde observations of

increasing tropospheric temperature and IWV during the winter season can coherently be explained by a change in atmospheric circulation resulting in increased atmospheric advection from lower latitudes towards the Svalbard region.

The variability of atmospheric circulation in the wintertime Northern hemisphere is dominated by the Arctic oscillation (AO) (Thompson and Wallace 1998), a see-saw of sea level pressure between the Arctic region and the mid-latitudes which shows an annular pattern. As the AO is strongly related to the strength of the polar vortex, it is also related to the variability in lower-tropospheric winds. In the positive (negative) AO phase, the sea level pressure is anomalously low (high) over the poles and high (low) over the surrounding lower-latitude zonal ring. A phase shift in the AO thus results in a change of the atmospheric mass exchange between the polar latitudes and the mid-latitudes, by modifying the zonal and meridional flow. For the last decade in years 2000 to 2007, a shift towards a meridional flow pattern has been found with anomalous geostrophic winds that tended to blow towards the central Arctic (Overland et al. 2008). Analysing the difference in daily AO indices between the periods 1993–2003 and 2004–2014, we also find a shift towards more negative AO indices. Furthermore, a recent increase of polar lows over the Greenland Sea–west of Svalbard–and over the Barents Sea has been found that may partly be explained by a change in the seasonal evolution of sea ice extent (Rojo et al. 2015).

While the wintertime temperature increase and wind direction changes in the free troposphere can conclusively be attributed to atmospheric large-scale circulation changes, additional factors have to be considered in the lowermost kilometre of the Ny-Ålesund atmospheric column. Throughout the year, the warming appears stronger in the boundary layer. Over the 22-year period, the boundary layer wind channelling has become more frequent. The vertical structure of the measured profiles suggests that the combination of boundary layer processes and complex topography lead to the formation of an inner fjord regime that is frequently decoupled from the free troposphere by a capping inversion above the surrounding mountain ridges. Processes potentially amplifying the tropospheric temperature increase in the boundary layer include changing properties in low-level clouds and a change in surface fluxes due to changes in ice and snow cover. The observed increase in winter IWV originates from an increase in the large-scale background humidity profiles but cannot unambiguously be attributed to long range transport. Though Park et al. (2015) show that downward longwave radiation increase in the Arctic is driven by horizontal moisture and warm air advection into the Arctic rather than by evaporation from the Arctic Ocean, the local conditions of fjord water surface may still have an impact. As the largest contribution to the water vapour column arises from the boundary layer, the winter humidity increase may also be

partly related to less ice cover on the fjord and/or higher sea surface temperature inducing more evaporation over the 22-year period. The water body of the fjord may further affect the heat flux to the atmosphere during the other months. Shorter snow cover periods during recent years (Maturilli et al. 2015) also affect the surface-atmosphere fluxes over the solid surface of the fjord environment, potentially contributing to the observed amplified boundary layer warming.

The combination with other operational instrumentation at the scientific super-site Ny-Ålesund (e.g. Doppler wind lidar, Eddy covariance, cloud ceilometer and others) will provide further insight to coupling processes between the surface and the atmosphere and between the boundary layer and the above troposphere. The long-term observations of the vertical distribution of temperature, humidity and wind by radiosondes allow the integration of measurements on smaller spatial and temporal scales in the broader climatic context. Towards the larger scale, the Ny-Ålesund atmospheric column climatology will help to place the peculiarities of the European Arctic among other regional characteristics within the Arctic climate system.

Acknowledgments The authors would like to thank the overwintering staff of the AWIPEV research base (former Koldewey station) in Ny-Ålesund for the devoted launches of thousands of radiosondes contributing to this study. Special thanks to Jürgen Graeser, Siegrid Debatin and Holger Deckelmann for technical hard- and software support. We also thank the GRUAN Lead Centre for reprocessing early Ny-Ålesund RS92 radiosonde data. Furthermore, we thank Sabine Erxleben and Dörthe Handorf for calculating AO patterns and indices and for helpful discussions during the review process. We thank the reviewers for their helpful comments.

References

- Beszczynska-Möller A, Fahrbach E, Schauer U, Hansen E (2012) Variability in Atlantic water temperature and transport at the entrance to the Arctic Ocean, 1997–2010. *ICES J Mar Sci* 69:852–863. doi:10.1093/icesjms/fss056
- Beine HJ, Argenti S, Maurizi A, Mastrantonio G, Viola A (2001) The local wind field at Ny-Ålesund and the Zeppelin mountain at Svalbard. *Meteorol Atmos Phys* 78:107–113. doi:10.1007/s007030170009
- Bintanja R, Graverson RG, Hazeleger W (2011) Arctic wintertime amplified by the thermal inversion and consequent low infrared cooling to space. *Nat Geosci* 4:758–761. doi:10.1038/NGEO1285
- Bodeker GE, Bojinski S, Cimini D, Dirksen RJ, Haeffelin M, Hannigan JW, Hurst DF, Leblanc T, Madonna F, Maturilli M, Mikalsen A, Philipona R, Reale T, Seidel DJ, Tan DGH, Thorne PW, Vömel H, Wang J (2016) Reference upper-air observations for climate: from concept to reality. *Bull Am Meteorol Soc* 97(1):123–135. doi:10.1175/BAMS-D-14-00072.1
- Chylek P, Folland CK, Lesins G, Dubey MK, Wang M (2009) Arctic air temperature change amplification and the Atlantic multidecadal oscillation. *Geophys Res Lett* 36:L14801. doi:10.1029/2009GL038777

- Curry JA, Schramm JL, Serreze MC, Ebert EE (1995) Water vapour feedback over the Arctic Ocean. *J Geophys Res* 100:14223–14229. doi:10.1029/95JD00824
- Dai A, Wang A, Thorne PW, Parker DE, Haimberger L, Wang X (2011) A new approach to homogenize daily radiosonde humidity data. *J Clim* 24:965–991. doi:10.1175/2010JCLI3816.1
- Devasthale A, Sedlar J, Tjernström M (2011) Characteristics of water-vapour inversions observed over the Arctic by Atmospheric Infrared Sounder (AIRS) and radiosondes. *Atmos Chem Phys* 11:9813–9823. doi:10.5194/acp-11-9813-2011
- Dirksen RJ, Sommer M, Immler FJ, Hurst DF, Kivi R, Vömel H (2014) Reference quality upper-air measurements; GRUAN data processing for the Vaisala RS92 radiosonde. *Atmos Meas Tech* 7:4463–4490. doi:10.5194/amt-7-4463-2014
- Doyle JG, Lesins G, Thackray CP, Perro C, Nott GJ, Duck TJ, Damoah R, Drummond JR (2011) Water vapour intrusions into the high Arctic during winter. *Geophys Res Lett* 38:L12806. doi:10.1029/2011GL047493
- Durre I, Vose RS, Wuertz DB (2006) Overview of the integrated global radiosonde archive. *J Clim* 19:53–68. doi:10.1175/JCLI3594.1
- Elliott WP, Gaffen DJ (1991) On the utility of radiosonde humidity archives for climate studies. *Bull Am Meteorol Soc* 72:1507–1520. doi:10.1175/1520-0477(1991)072<1507:OTUORH>2.0.CO;2
- Esau I, Ripina I (2012) Wind climate in Kongsfjorden, Svalbard, and attribution of leading wind driving mechanisms through turbulence-resolving simulations. *Adv Meteorol ID568454*. doi:10.1155/2012/568454
- Francis JA, Hunter E (2006) New insight into the disappearing Arctic sea ice. *EOS Trans Am Geophys Union* 87:509–511
- Gaffen DJ (1994) Temporal inhomogeneities in radiosonde temperature records. *J Geophys Res* 99:3667–3676. doi:10.1029/93JD03179
- Graversen RG, Mauritsen T, Tjernström M, Källén E, Svensson G (2008) Vertical structure of recent Arctic warming. *Nature* 451:53–56. doi:10.1038/nature06502
- Gruber C, Haimberger L (2008) On the homogeneity of radiosonde wind time series. *Meteorol Z* 17:631–643. doi:10.1127/0941-2948/2008/0298
- Hannachi A, Jolliffe IT, Stephenson DB (2007) Empirical orthogonal functions and related techniques in atmospheric science: a review. *Int J Climatol* 27:1119–1152. doi:10.1002/joc.1499
- Hansen J, Nazarenko L (2004) Soot climate forcing via snow and ice albedos. *Proc Natl Acad Sci U S A* 101:423–428. doi:10.1073/pnas.2237157100
- Hare FK (1960) The summer circulation of the arctic stratosphere below 30 km. *Q J R Meteorol Soc* 86:127–143
- Hyland RW, Wexler A (1983) Formulations for the thermodynamic properties of the saturated phases of H₂O from 173.15 K to 473.15 K. *ASHRAE Trans* 89(2 A):500–519
- Kahl JD (1990) Characteristics of the low-level temperature inversion along the Alaskan Arctic Coast. *Int J Climatol* 10:537–548. doi:10.1002/joc.3370100509
- Kivi R, Kujanpää J, Aulamo O, Hassinen S, Heikkinen P, Calbet X, Montagner F, Vömel H (2009) Observations of water vapor profiles over Northern Finland by satellite and balloon borne instruments. Proceedings of the 2009 EUMETSAT Meteorological Satellite Conference, EUMETSAT P.55, ISSN 1011-3932.
- Lanzante JR (1996) Resistant, robust and non-parametric techniques for the analysis of climate data: theory and examples including applications to historical radiosonde station data. *Int J Climatol* 16:1197–1226. doi:10.1002/(SICI)1097-0088(199611)16:11<1197::AID-JOC89>3.0.CO;2-L
- Marks AA, King MD (2013) The effects of additional black carbon on the albedo of Arctic sea ice: variation with sea ice type and snow cover. *Cryosphere* 7:1193–1204. doi:10.5194/tc-7-1193-2013
- Massoli P, Maturilli M, Neuber R (2006) Climatology of Arctic polar stratospheric clouds as measured by lidar in Ny-Ålesund, Spitsbergen (79°N, 12°E). *J Geophys Res* 111:D09206. doi:10.1029/2005JD005840
- Maturilli M, Neuber R, Massoli P, Cairo F, Adriani A, Moriconi ML, Di Donfrancesco G (2005) Differences in Arctic and Antarctic PSC occurrence as observed by lidar in Ny-Ålesund (79°N, 12°E) and McMurdo (78°S, 167°E). *Atmos Chem Phys* 5:2081–2090
- Maturilli M, Herber A, König-Langlo G (2013) Climatology and time series of surface meteorology in Ny-Ålesund, Svalbard. *Earth Syst Sci Data* 5:155–163. doi:10.5194/essd-5-155-2013
- Maturilli M, Herber A, König-Langlo G (2015) Surface radiation climatology for Ny-Ålesund, Svalbard (78.9°N), basic observations for trend detection. *Theor Appl Climatol* 120:331–339. doi:10.1007/s00704-014-1173-4
- Miloshevich LM, Vömel H, Paukkunen A, Heymsfield AJ, Oltmans SJ (2001) Characterization and correction of relative humidity measurements from Vaisala RS80-A radiosondes at cold temperatures. *J Atmos Ocean Technol* 18:135–155
- Miloshevich LM, Paukkunen A, Vömel H, Oltmans S (2004) Development and validation of a time-lag correction for Vaisala radiosonde humidity measurements. *J Atmos Ocean Technol* 21:1305–1327. doi:10.1175/1520-0426(2004)021<1305:DAVOAT>2.0.CO;2
- Moradi I, Soden B, Ferraro R, Arkin P, Vömel H (2013) Assessing the quality of humidity measurements from global operational radiosonde sensors. *J Geophys Res* 118:8040–8053. doi:10.1002/jgrd.50589
- Nygård T, Valkonen T, Vihma T (2014) Characteristics of Arctic low-tropospheric humidity inversions based on radio soundings. *Atmos Chem Phys* 14:1959–1971. doi:10.5194/acp-14-1959-2014
- Ohmura A (2001) Physical basis for the temperature-based melt-index method. *J Appl Meteorol* 40:753–761. doi:10.1175/1520-0450(2001)040<0753:PBFTTB>2.0.CO;2
- Overland JE, Wang M, Salo S (2008) The recent Arctic warm period. *Tellus A* 60:589–597. doi:10.1111/j.1600-0870.2008.00327.x
- Park DSR, Lee S, Feldstein SB (2015) Attribution of the recent winter sea ice decline over the Atlantic sector of the Arctic Ocean. *J Clim* 28:4027–4033. doi:10.1175/JCLI-D-15-0042.1
- Preisendorfer RW (1988) Principal component analysis in meteorology and oceanography. In: Developments in atmospheric science, vol 17. Elsevier, Amsterdam
- Rojo M, Claud C, Mallet PE, Noer G, Carleton AM, Vicomte M (2015) Polar low tracks over the Nordic Seas: a 14-winter climate analysis. *Tellus A* 67:24660. doi:10.3402/tellusa.v67.24660
- Scherhag R (1952) Die explosionsartige Stratosphärenwärmung des Spätwinters 1951/52. *Ber Deut Wetterdienst* 38:51–63
- Schweiger AJ, Lindsay RW, Vavrus S, Francis JA (2008) Relationships between Arctic sea ice and clouds during autumn. *J Clim* 21:4799–4810. doi:10.1175/2008JCLI2156.1
- Screen JA, Simmonds I (2010) The central role of diminishing sea ice retreat in recent Arctic temperature amplification. *Nature* 464:1334–1337. doi:10.1038/nature09051
- Sedlar J, Tjernström M (2009) Stratiform cloud - inversion characterization during the Arctic melt season. *Bound-Layer Meteorol* 132:455–474. doi:10.1007/s10546-009-9407-1
- Sedlar J, Shupe MD, Tjernström M (2012) On the relationship between thermodynamic structure and cloud top, and its climate significance in the Arctic. *J Clim* 25:2374–2393. doi:10.1175/JCLI-D-11-00186.1
- Serreze MC, Barrett AP, Stroeve JC, Kindig DN, Holland MM (2009) The emergence of surface-based Arctic amplification. *Cryosphere* 3:11–19. doi:10.5194/tc-3-11-2009
- Serreze MC, Barry RG (2011) Processes and impacts of Arctic amplification: a research synthesis. *Glob Planet Chang* 77:85–96

- Serreze MC, Barrett AP, Cassano JJ (2011) Circulation and surface controls on the lower tropospheric air temperature field of the Arctic. *J Geophys Res* 116:D07104. doi:[10.1029/2010JD015127](https://doi.org/10.1029/2010JD015127)
- Shindell D, Faluvegi G (2009) Climate response to regional radiative forcing during the twentieth century. *Nat Geosci* 2:294–300. doi:[10.1038/NGEO473](https://doi.org/10.1038/NGEO473)
- Shupe MD, Intrieri JM (2004) Cloud radiative forcing of the Arctic surface: the influence of cloud properties, surface albedo, and solar zenith angle. *J Clim* 17:616–628. doi:[10.1175/1520-0442\(2004\)017<0616:CRFOTA>2.0.CO;2](https://doi.org/10.1175/1520-0442(2004)017<0616:CRFOTA>2.0.CO;2)
- Soden BJ, Lanzante RL (1996) An assessment of satellite and radiosonde climatologies of upper-tropospheric water vapor. *J Clim* 9:1235–1250. doi:[10.1175/1520-0442\(1996\)009<1235:AAOSAR>2.0.CO;2](https://doi.org/10.1175/1520-0442(1996)009<1235:AAOSAR>2.0.CO;2)
- Solomon A, Shupe MD, Persson POG, Morrison H (2011) Moisture and dynamical interactions maintaining decoupled Arctic mixed-phase stratocumulus in the presence of a humidity inversion. *Atmos Chem Phys* 11:10127–10148. doi:[10.5194/acp-11-10127-2011](https://doi.org/10.5194/acp-11-10127-2011)
- Thompson DWJ, Wallace JM (1998) The Arctic Oscillation signature in the wintertime geopotential height and temperature fields. *Geophys Res Lett* 25:1297–1300
- Trefffeisen R, Krejci R, Ström J, Engvali AC, Herber A, Thomason L (2007) Humidity observations in the Arctic troposphere over Ny-Ålesund, Svalbard based on 15 years of radiosonde data. *Atmos Chem Phys* 7:2721–2732. doi:[10.5194/acp-7-2721-2007](https://doi.org/10.5194/acp-7-2721-2007)
- Vihma T, Kilpeläinen T, Manninen M, Sjöblom A, Jakobson E, Palo T, Jaagus J, Maturilli M (2011) Characteristics of temperature and humidity inversions and low-level jets over Svalbard fjords in spring. *Adv Meteorol* 2011:ID486807. doi:[10.1155/2011/486807](https://doi.org/10.1155/2011/486807)
- Wang J, Cole HL, Carlson DJ, Miller ER, Beierle K (2002) Corrections of humidity measurement errors from the Vaisala RS80 radiosonde—application to TOGA COARE data. *J Atmos Ocean Technol* 19:981–1002. doi:[10.1175/1520-0426\(2002\)019<0981:COHMEF>2.0.CO;2](https://doi.org/10.1175/1520-0426(2002)019<0981:COHMEF>2.0.CO;2)
- Woods C, Caballero R (2016) The role of moist intrusions in winter Arctic warming and sea ice decline. *J Clim*. doi:[10.1175/JCLI-D-15-0773.1](https://doi.org/10.1175/JCLI-D-15-0773.1)
- World Meteorological Organization (1957) Meteorology—a three dimensional science. *WMO Bull* 6:134–138
- Zängl G, Hoinka KP (2001) The tropopause in the polar regions. *J Clim* 14:3117–3139
- Zhang Y, Seidel DJ (2011) Challenges in estimating trends in Arctic surface-based inversions from radiosonde data. *Geophys Res Lett* 38:L17806. doi:[10.1029/2011GL048728](https://doi.org/10.1029/2011GL048728)